-RESEARCH PAPER-

International Journal of Mining and Geo-Engineering

IJMGE

IJMGE 58-2 (2024) 145-152

DOI: 10.22059/IJMGE.2024.366296.595103

Examining removal or reduction of suction on displacement, separation of particles and energy consumption of jig by coupling computational fluid dynamics (CFD) and discrete element method (DEM)

Seyed Amir Rastialhosseini [a] and Ali Akbar Abdollahzadeh [b, *]

[a] *Department of Mining engineering, University of Kashan, Kashan, Iran.*

[b] *Faculty of Mining Engineering, Amirkabir University of Technology, Tehran, Iran.*

Article History:

Received: 06 October 2023.

Revised: 12 December 2023.

Accepted: 09 January 2024.

ABSTRACT

The effect of removing suction on energy consumption, displacement, and separation of particles with different sizes and densities in the jig was investigated by CFD-DEM coupling. Water velocity functions were categorized into four modes: normal sinusoidal, partial removal of suction, complete removal of suction, and optimal. Particles rise to a certain height in the normal sinusoidal mode, while their jump height increases in the case of partial or complete removal of suction. The jump was controlled by fluid and added (Hutch) water velocities. Increasing the maximum jump height of particles leads to a decrease in separation, an increase in operational costs, and heightened particle mixing and energy consumption. In both modes of partial or complete suction removal, the fluid velocity should be reduced. The extent of velocity reduction depends on the power required to move the particles. The simulation of coarse particles (7 and 8 mm) revealed that in the complete removal of suction, the velocity should be decreased to less than half of the normal sinusoidal mode, and the hutch water velocity should be equivalent to the velocity amplitude. The energy consumption for the optimal mode was significantly lower than that of the other modes.

Keywords: *Jigging, Particle trajectory, Suction removing, Water velocity function.*

1. Introduction

The jig separates minerals based on different specific gravities by a stream of oscillating water. The jig operates based on expanding the minerals embedded in the bed, so that the heavier and smaller particles penetrate the bed spaces and the particles with high specific gravity settle into conditions that are likely similar to hindered settling [1].

In the jig operation, sufficient energy should be provided to the liquid so that the particles reach full expansion. Heavier and coarser particles require a stronger lifting force, which must be provided by the fluid velocity and its amplitude. Factors influencing the operation include the volume of water on the top of the bed, the horizontal cross-section, the velocity of the water moving back and forth, the maximum water velocity achieved in each stage of the cycle, and the maximum height of the water obtained due to the maximum water velocity [2].

The water velocity profile is expressed as a sinusoidal function with a period of T [3]. This function must satisfy two crucial criteria for separation: firstly, it must elevate the bed enough to allow continuous expansion and loosening, and secondly, it must provide enough time for the particles to rearrange.

In a feed, heavy particles may struggle to penetrate the bed and could be placed in the path of low-density particles, resulting in loss. Adding hutch water (additional water) from the bed to the top reduces the bed's compaction, thereby reducing suction and its duration. Introducing a significant amount of water may eliminate suction, causing particles to fall only under the initial acceleration and density effect. However, this could increase the loss of fine particles due to the extended pulsion time and increased upward flow velocity [1].

Various parameters are examined to evaluate the performance of the jigging machine, including separation speed, the number of cycles to achieve separation, and energy input. Different methods, such as starting the next oscillation as soon as particles reach the bottom of the bed or adding hatch water, have been proposed to reduce energy consumption [4,5].

Numerous theories have been proposed to describe the jigging process [6], involving experimental models, including the potential energy model [7,8], numerical models, such as two-dimensional and three-dimensional discrete element methods (DEM) [6,9-14], CFD models [15-18], and CFD-DEM [4,5,19,20]. Additionally, Monte Carlo Potential Energy [21], Neural Network Models [22], and Statistical Models [23] have been explored. These models evaluate the impact of two-way coupling, porosity, and hydrodynamic forces on jig performance.

The coupling of computational fluid dynamics and the discrete element method (CFD-DEM) has been employed to simulate the behavior of solid particles in a separator, with particle trajectories analyzed [24]. Although the CFD-DEM is limited in simulating a large number of particles, methods such as the coarse-grain method have been proposed to address this limitation [25]. Two-way coupling considers the effects of the dispersed phase on the continuous phase and vice versa, including displacement, momentum between phases, mass, and heat transfer [26].

* Corresponding author. *Fax/Tel*: +98-3155912420, *E-mail address:* : abdzad@aut.ac.ir (A. A. Abdollahzadeh).

Previous studies using the CFD-DEM coupling method have examined the initial feed with mono-size and two densities [4,5,19], two particles with the same terminal settling velocity [19], and mono-size with four densities [20]. In this approach, particle-particle and particle-wall interactions are considered.

However, the effect of removing suction on the jig performance and energy consumption has not been investigated using the CFD-DEM coupling method. This study examines particle trajectory and energy consumption for different water velocity function modes (normal sinusoidal, partial suction removal, complete suction removal, and optimal) using the CFD-DEM method to simulate jigging performance for particles with different sizes and densities. The study specifically investigates the effect of complete removal of suction on the velocity function, employing CFD and DEM modelling in three dimensions (3D).

2. Simulation methods

2.1. governing equations

The CFD-DEM model has been described in several articles [4,5,19,20]. However, the general sequence of governing equations is described. The solid phase is considered a discrete phase and solved using the DEM. The translational and rotational motion of a particle at any time, t, in the bed is determined by the Newton's second law of motion.

$$m_i(dv_i/dt) = f_{f,i} + \sum_{j=1}^{k_i}\left(f_{c,ij} + f_{d,ij}\right) + f_{g,i} \quad (1)$$

$$I_i(d\omega_i/dt) = \sum_{j=1}^{k_i} T_{IJ} \quad (2)$$

where m_i, I_i, k_i, V_i, and ω_i are the mass, moment of inertia, number of particles in contact, speed of transfer, and rotation of the i^{th} particle, and $f_{f,i}$ and $f_{g,i}$ are the fluid drag force and gravitational force, respectively. The variables $f_{c,ij}$, $f_{d,ij}$ and T_{ij} are the contact force, viscous contact damping force, and torque between particles i and j, respectively. These interparticle forces and torques accumulate on particle k_i in contact with particle i.

In the ESSS Rocky 4.5.2 software package, various drag correlations based on particle shape (spherical and non-spherical) and particle concentration (dilute or dense flows) are available. Here, the drag law is used for spherical particles and dense flow, and the particle-fluid interaction force is calculated using the drag force correlation of Di Felice [27]. The particle-particle and particle-wall contact forces are based on the soft sphere method. The liquid phase is treated as a continuous phase moving in a porous medium created by the particles and is modeled similarity to the conventional two-fluid model, where the porosity (or liquid volume fraction) modifies the standard single-phase Navier-Stokes equations. The governing equations are the conservation of mass and momentum in terms of local average variables on a computational cell, which is defined by ESSS Rocky [28]:

$$\frac{\partial(\alpha_f \rho_f)}{\partial t} + \nabla.\left(\alpha_f \rho_f u\right) = 0 \quad (3)$$

$$\frac{\partial(\alpha_f \rho_f u)}{\partial t} + \nabla.\left(\alpha_f \rho_f uu\right) = -\alpha_f \nabla P - \frac{\sum_{i=1}^{k_c} f_{f,i}}{\Delta V} + \nabla\left(\alpha_f \tau\right) + \alpha_f \rho_f g + F_{P\to f} \quad (4)$$

where ρ_f, u, and P are the fluid density, velocity, and pressure, respectively. τ, α_f, and ΔV are the fluid viscous stress tensors, porosity fluid volume fraction, and volume of a computational cell, respectively. $F_{P\to f}$ represents the source term of momentum from interaction with the particulate phase.

The particle flow is numerically solved by the discrete element modelling (DEM) using the ESSS Rocky 4.5.2 software package. Using the DEM simulation, it is possible to run simulations of millions of particles with complex shapes and interparticle forces [29]. The continuous liquid phase is solved using the Computational Fluid Dynamics (CFD) and the commercial software package ANSYS FLUENT 2020 R2. The two-way coupling between the DEM and CFD is achieved. The way in which coupling is implemented allows both solvers to work in parallel, using N processors for the fluid phase solution and M processors for the particulate phase solution (or using the GPU processing to solve the DEM part). The following operations are performed during the particulate system solution: 1. The DEM solver time step calculation, 2. Initial fluid flow field calculation (velocity, pressure, and physical properties) on the CFD solver and transfer to the DEM solver, 3. Particulate phase volume fraction and initial interaction terms calculation (interaction forces and heat transfer rates) on the DEM solver and transfer to the CFD solver, 4. The CFD solver time step correction in order to have an integer multiple of the DEM solver time step. 5. Initial solid phase field update on the CFD solver, 6. Parallel execution of one CFD solver time step and n DEM solver time steps, 7. Semi-implicit transfer of the interaction forces from the DEM solver to the CFD solver, 8. Velocity, pressure, and physical properties in each cell transfer from the CFD solver to the DEM solver, and 9. Repetition of the process until reaching the total simulation time [28].

2.2. Simulation conditions

The 3D model includes a rectangular cubic domain with dimensions of 0.06 × 0.04 × 0.5 meters, which is filled with spherical particles with diameters of 7 and 8 mm in 3 densities of 2700, 3400, and 4400 kg/m^3 and liquid. The liquid is water with a density of 1000 kg/m^3. In Rocky package, the CFD-DEM coupling method has been developed for the ideal case in which the particles are smaller than the CFD cells. In the CFD solver, the CFD cells are considered with dimensions of 0.02 × 0.02 × 0.02 meters, and the flow is selected turbulent. The type of viscous model is the standard k-ε. In the k-ε model, the assumption is that the flow is fully turbulent, and the effects of molecular viscosity are negligible. The standard k-ε model is therefore valid only for fully turbulent flows [30]. The solid fraction, interaction forces, and exchanged heat amounts are covered by the mapped information from the DEM to the CFD. Rocky provides two options to perform this mapping: uniform distribution and volumetric diffusion [28]. In this study, the volumetric diffusion method is used, and the reader can refer to the Rocky Manual for more details.

In calculating the time-dependent movement of particle and fluid phases, different time steps are used in the CFD and DEM simulations [31]. According to Table 1, there are six types of particles in different sizes and densities. The densities of 2700, 3400, and 4400 kg/m^3 are indicated by numbers 1, 2, and 3, respectively. For example, particle 2-7 is characterized by a particle with a density of 3400 kg/m^3 and a size of 7 mm. 160 of each particle and a total of 960 particles are used in each test. The characterizations of the CFD and DEM are listed in Table 2.

The bottom inlet is considered a wall for the particle phase, so the particles cannot go down from it, but it is an inlet for the liquid. The upper outlet is considered to have zero normal gradient opening conditions. The side walls are considered with no-slip boundary conditions. Water is injected through the inlet upwards in a vertical direction and the inlet flow is sinusoidalized to produce a sinusoidal oscillation profile using a user-defined function. The fluid flow and DEM modelling of the particles are considered in three dimensions (3D).

The sinusoidal velocity function is as follows [3,32]:

$$U(t) = (2\pi/T)L\sin\left((2\pi/T)t\right) \quad (5)$$

where $U(t)$, T, L, and t are the velocity over time (m/s), cycle time (s), half of the displacement (m), and time (s), respectively. To remove or reduce suction, the velocity function is based on Eq. (6):

Table 1. Naming six types of particles with different sizes and densities.

Particles		Particle Size	
		7 mm	**8** mm
Material	**1** (2700 Kg/m^3)	1_7	1_8
	2 (3400 Kg/m^3)	2_7	2_8
	3 (4400 Kg/m^3)	3_7	3_8

Table 2. The characterization of the CFD and DEM.

Particle phase (DEM)		Liquid phase (CFD)		
Particle density (kg m^{-3})	2700, 3400, 4400	Viscosity (kg m^{-1} s^{-1})		1*10^{-3}
Particle diameter (mm)	7,8	Density (kg m^{-3})		1000
Young's modulus (Nm^{-2})	1*10^{8}	CFD cell	Length (m)	0.02
Poisson ratio (Nm^{-2})	0.3		Width (m)	0.02
			Height (m)	0.02
		Bed geometry	Length (m)	0.06
			Width (m)	0.04
			Height (m)	0.5
Time step (s)	By Rocky	Time step (s)		5*10^{-3}

$$U(t) = U_h + U_0 \sin((2\pi/T)t) \quad (6)$$

where $U(t)$, U_h, U_0, T, and t are the velocity function over time, additional water velocity (hutch water), velocity amplitude, cycle time, and time, respectively.

Preliminary parameters of the sinusoidal velocity function, including velocity amplitudes of 0.2, 0.3, 0.35, and 0.4 m/s and cycle times of 1, 1.5, and 2 seconds were tested. The mode that has the complete separation of particles in the lowest cycle (that is, the velocity amplitude of 0.35 (m/s) and the cycle time of 1.5 (s)) was chosen as the basis for the sinusoidal mode.

Four modes, including the normal sinusoidal, partial removal of suction, complete removal of suction, and optimal velocity function with Eqs. (7)-(10) are shown in Fig. 1. The optimal velocity function is defined by having two criteria. Firstly, it enables the movement of particles and water above the particles, and second, having maximum separation with minimum energy consumption while having the least number of cycles. This optimal function is obtained by repeated tests and changing the velocity amplitude and hutch water compared to the initial normal sinusoidal state. Among the tests with the velocity amplitude and hutch water of 0.1, 0.15, and 0.2m/s, the optimal mode was selected with a velocity amplitude and hutch water of 0.15.

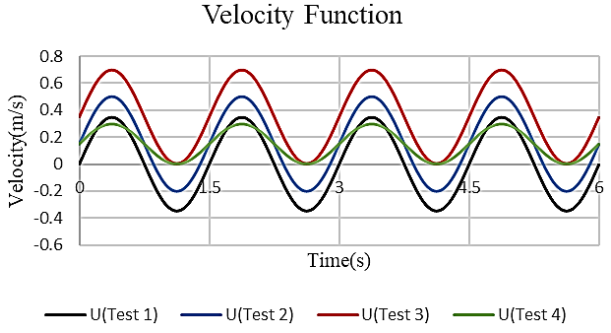

Figure 1. Velocity functions used in the study.

The simulation starts with a random generation of non-overlapping particles, followed by a period of gravitational settling to form a fixed bed of the initial mixture. During the bed formation, the buoyancy force of the particles is turned off to prevent segregation and achieve better packing of the mixture before the jigging begins. After bed formation, the liquid is injected from the bottom with a specific oscillating profile and the jigging begins.

The water velocity function is checked in three modes, including: the normal sinusoid, partial removal of suction and complete removal of suction.

$$U(t) = 0.0 + 0.35\sin((2\pi/1.5)t) \quad (7)$$

$$U(t) = 0.15 + 0.35\sin((2\pi/1.5)t) \quad (8)$$

$$U(t) = 0.35 + 0.35\sin((2\pi/1.5)t) \quad (9)$$

Then, to completely remove the suction, the optimal conditions of the water velocity function according to formula (10) are considered and compared with:

$$U(t) = 0.15 + 0.15\sin((2\pi/1.5)t) \quad (10)$$

2.3. Energy Consumption and states of tests

Various parameters to judge the performance of a jigging device are the separation speed, number of cycles to achieve concentration, final degree of separation, and energy input [4,5]. The following formula is used to calculate the input power and energy consumption:

$$Q = U(t)*A \quad (11)$$

$$Power = \Delta p*Q \quad (12)$$

$$E = power*\Delta t_{CFD} \quad (13)$$

Where, Q, U(t), A, Δp, E, and Δt_{CFD} are the volumetric flow rate, fluid velocity, cross-sectional area of the domain, total pressure drops, energy consumption, and time step of ANSYS, respectively. The fluid velocity, U(t), at the inlet of the computational domain is calculated based on formulas (7-10) and the total pressure drop is a summation of various pressure drops due to the fluid acceleration, particle acceleration, fluid-to-wall friction, solid-to-wall friction, static head of solids, and static head of fluid. The contributions of wall effects are not resolved due to the computational effort and complexity. These formulas (11-13) were used for all tests.

3. Computational tests with CFD and DEM coupling

3.1. Average position of particles with the same density

Computational tests were carried out based on Eqs. (7)-(10), and labelled as Test 1 to 4, respectively. The average heights of different particles as a function of time are shown in Figs. 2-5. The average position of the materials shows complete or partial separation and non-separation in successive cycles. In all tests, the computational domain (column dimensions), computational cell, and time step are the same. The weight of particles in all states is 1.1315 kg. The velocity function should be able to move particles and water above it. The separation is considered complete if the average height of particles with the same density does not change at three cycles. Rocky shows the trajectory of particles and average height of particles with the same density. The actual simulation time for different tests ranges from 12 to 22 hours. The multiple processors are Intel(R) Core (TM) i7-9750H CPU @ 2.60GHz and 8.00 GB RAM. The results of the average position, the maximum height in jump, the minimum height in suction, and the average displacement range of particles with the same density in four tests are shown in Table 3.

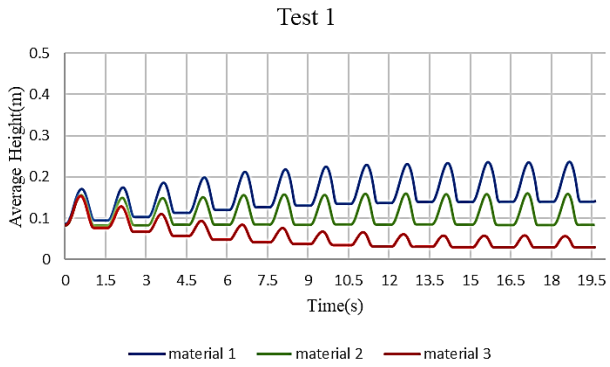

Figure 2. The average position of material (particles based on the same density) over time with the water velocity function of Eq. (7).

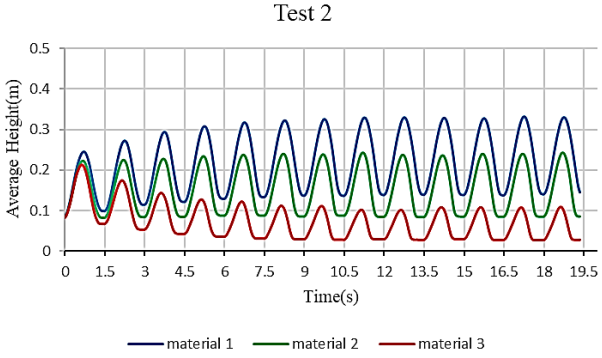

Figure 3. The average position of material (particles based on the same density) over time with the water velocity function of Eq. (8).

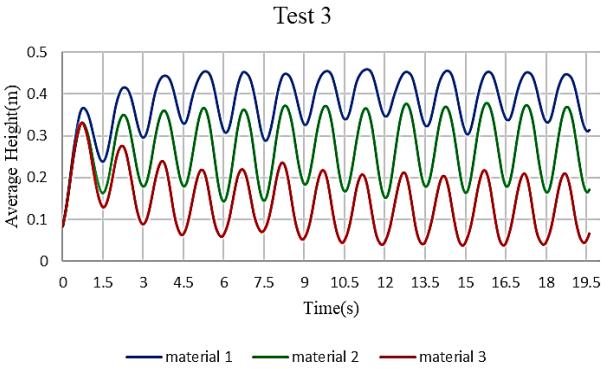

Figure 4. The average position of material (particles based on the same density) over time with the water velocity function of Eq. (9).

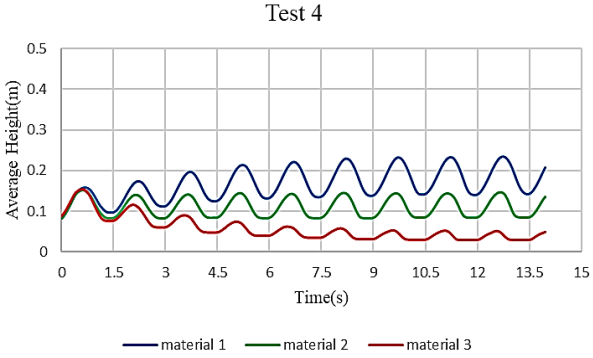

Figure 5. The average position of material (particles based on the same density) over time with the water velocity function of Eq. (10).

Table 3. The characteristic values of the water velocity function, average position, and range of movement of materials.

Characterization		Test 1	Test 2	Test 3	Test 4
Water Velocity Function (m/s)		$U(t) = 0.0 + 0.35\sin((2\pi/1.5)t)$	$U(t) = 0.15 + 0.35\sin((2\pi/1.5)t)$	$U(t) = 0.35 + 0.35\sin((2\pi/1.5)t)$	$U(t) = 0.15 + 0.15\sin((2\pi/1.5)t)$
Hutch Water Velocity, U_h(m/s)		0	0.15	0.35	0.15
Velocity Amplitude, U_0(m/s)		0.35	0.35	0.35	0.15
Cycle Time, T(s)		1.5	1.5	1.5	1.5
Frequency, f(1/min)		40	40	40	40
Initial Particle gravity center/Domain heigh(m)		0.085/0.5	0.085/0.5	0.085/0.5	0.085/0.5
Average at max. pulsion	Material 1	0.235	0.33	0.45	0.235
	Material 2	0.16	0.24	0.37	0.145
	Material 3	0.06	0.11	0.21	0.055
Average at min. pulsion	Material 1	0.14	0.14	0.33	0.14
	Material 2	0.085	0.085	0.17	0.085
	Material 3	0.03	0.03	0.04	0.03
Movement range	Material 1	0.095	0.19	0.12	0.095
	Material 2	0.075	0.155	0.2	0.06
	Material 3	0.03	0.08	0.17	0.025

Figures 2-5 show the average positions of light, medium, and heavy particles at different times. Considering that the cycle time is 1.5 seconds, in some cases, a long-term stoppage is observed on the bottom of the bed. According to Table 3, the mobility of heavy particles in the normal sinusoidal mode (by 0.03 m) is less than the complete and partial removal of suction modes (by 0.17 and 0.08 m, respectively) and more than the optimal mode (0.025).

3.2. Average position of particles based on size and densities

The height of the six particles described in Table 1, based on Eqs. (7)-(10), are displayed in Figs. 6-9. In Figs. 6 and 9, which are related to the perfect sinusoidal mode (Test 1) and the optimal mode (Test 4), the complete separation of six particles based on density and size is observed. In Figs. 7 and 8 related to Test 2 and 3, there is a small amount of mixing of heavy and medium particles.

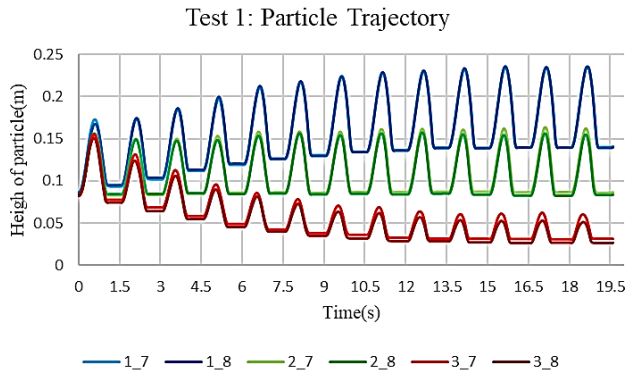

Figure 6. The average position of particles based on size and density over time with the water velocity function of Eq. (7).

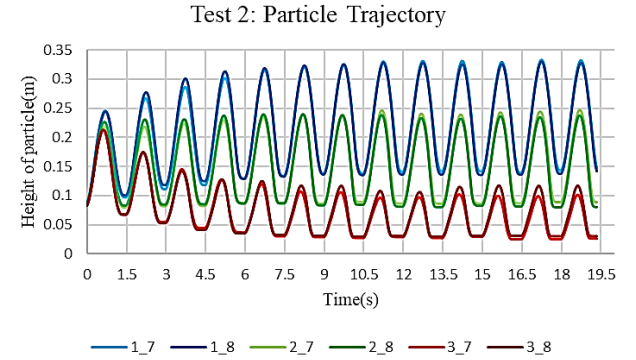

Figure 7. The average position of particles based on size and density over time with the water velocity function of Eq. (8).

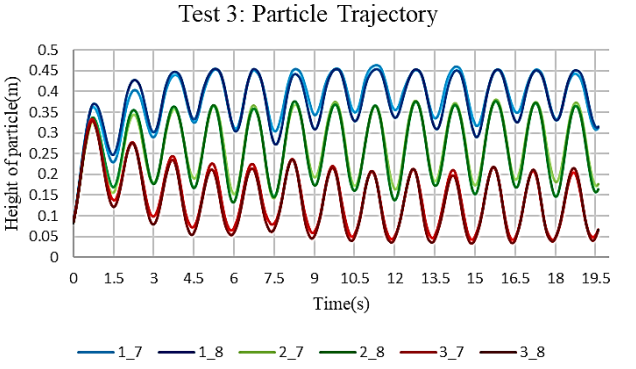

Figure 8. The average position of particles based on size and density over time with the water velocity function of Eq. (9).

3.3. Energy consumption

There are different ways to check the performance of the jig. These methods are generally based on the jig theories. In addition to separation speed, the number of cycles required to achieve separation, grade, and recovery, energy consumption is also an important aspect. In this study, the work of Viduka [4,5] was used to check the energy consumption. According to Fig. 10, under optimal conditions (Test 4), the energy consumption is the lowest, and the mode of complete removal of suction with high velocity amplitude (Test 3) has the highest energy consumption.

4. Observations, discussion, and validation

4.1. Observation and discussion

Figure 2 relates to Test 1. In this test, the water velocity function is based on Eq. (7) and the specifications are: U_0=0.35, U_h=0.0, T=1.5, f=40. The stopping of all three types of particles at the bottom of the bed is observed after complete settling for 0.45 s of the 1.5 second cycle time. Therefore, according to the stop time, it is possible to reduce the cycle time in this mode (normal sinusoidal). By reducing the cycle time, the speed of recovery increases, but the reduction of the cycle time increases the frequency and is economically significant.

Figure 3 relates to Test 2. In this test, the water velocity function is based on Eq. (8) and the specifications are: U_0=0.35, U_h=0.15, T=1.5, f=40. As can be seen, with the addition of hutch water (in other words, removing part of the suction, U_h=0.15), the stopping time at the bottom of the bed decreases. But the stopping time is still significant for particles with medium and heavy densities and partial mixing of particles with medium and heavy densities is observed until the end of all cycles. In this test, heavy particles stop for 0.45 out of 1.5 seconds, medium particles for 0.3 out of 1.5 seconds, and light particles for 0.1 out of 1.5 seconds at the bottom of the bed.

Figure 4 relates to Test 3. In this test, the water velocity function is based on Eq. (9) and the specifications are: U_0=0.35, U_h=0.35, T=1.5, f=40. Stopping of particles is not observed at the bottom of the bed, but the light particles stop at the maximum height for 0.2 out of 1.5 second cycle time. The high amount of hutch water (U_h=0.35) causes the high turbulence of light particles and instability of their maximum and minimum heights. A small amount of instability is also observed for medium and heavy particles. Therefore, in the case of complete removal of suction, the amplitude of velocity function (U_0) and hutch water (U_h) should be reduced by an appropriate amount to prevent disturbance.

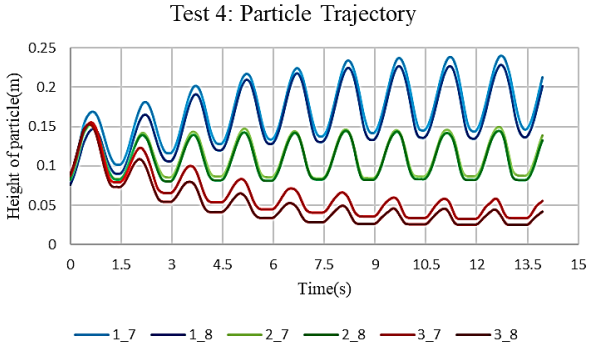

Figure 9. The average position of particles based on size and density over time with the water velocity function of Eq. (10)

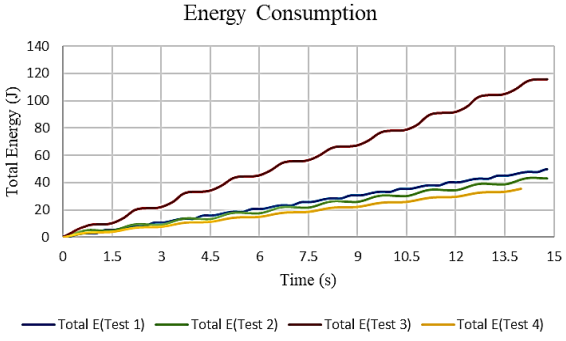

Figure 10. The energy consumption graph for four tests.

Figure 5 relates to test 4. In this test, the water velocity function is based on Eq. (10) and the specifications are: U_0=0.15, U_h=0.15, T=1.5, f=40. It is called the optimal test to completely remove suction by reducing the velocity amplitude. Under optimal conditions, after four cycles, materials with the same density move completely separately and are separated. Figs. 11 and 12 show the position of particles based on particle size and density, respectively.

Comparing Test 1 (normal sinusoidal mode) with Test 3 (sinusoidal mode with complete removal of suction) shows that with the same velocity amplitude (U_0) in the complete removal of suction mode (U_h=0.35), there is a stoppage of light particles at the maximum height of the computational domain, which means that if the height of the domain was greater than this value, the particles would rise higher. Therefore, in the complete removal of suction mode, the velocity amplitude must be reduced so that the particles travel less upward.

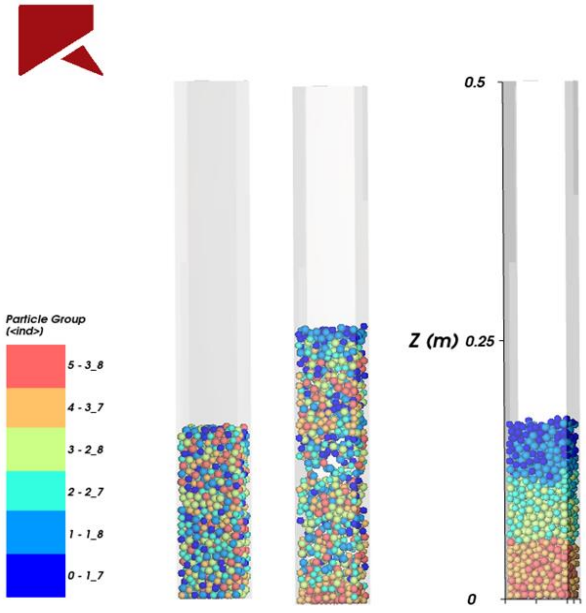

Figure 11. The position of particles obtained by the ESSS ROCKY on three dimensions based on particle size and densities (named at Table 1), left to right: t=0, t=2.25, t=13.5 s.

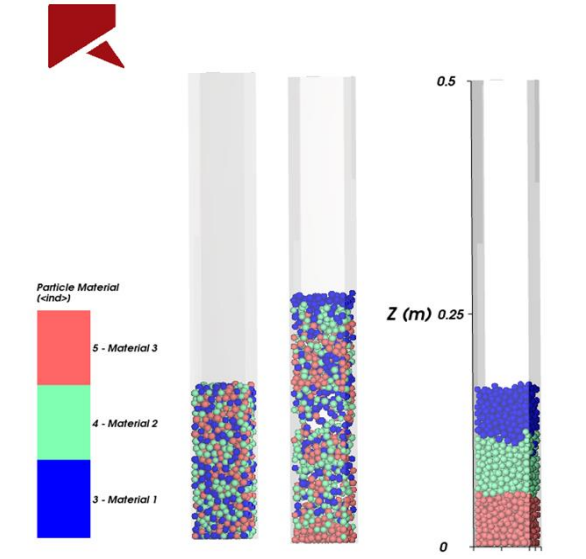

Figure 12. The position of particles obtained by the ESSS ROCKY on three dimensions based on material (named at Table 1), left to right: t=0, t=2.25, t=13.5 s.

The review of four Tests shows that the optimal mode of complete suction removal has the best results compared to the other modes and has similar results to the normal sinusoidal mode. In the complete removal of suction mode compared to the normal sinusoidal mode (without removal of suction), the velocity amplitude is changed and reduced. Hutch water is selected to be equivalent to the velocity amplitude, while the suction is completely removed and the lifting force of the particles is provided with hutch water.

According to Table 3, while the amplitude and frequency of the velocity function remain constant, the increase of hutch water increases the maximum jump of particles. In the complete removal of suction mode, the particles would rise to the maximum height and if the domain was higher, they would still rise higher.

The height of the water on the particles affects both the rate at which particles rise and their maximum height during the pulsation stage. The reason is that the velocity function must have the ability to lift both the particles and water on them.

The stoppage of particles at the bottom of the bed or the maximum height of the domain is clearly evident from the particle position graphs in the form of widening of both the lowest and highest points so that these points lose sharpness and tend to broaden.

Figures 6-9 show that if the suction is completely removed and the velocity amplitude does not decrease compared to the normal sinusoidal mode (without suction removal), while consuming more energy, the particles will rise to the highest point and stop there for a while, and with the reduction of separation caused by remixing. In other words, high velocity disrupts the stratification, arrangement, and placement of particles, and mixing may occur.

It is important to note that if the initial feed has a wide variety of sizes and densities, removing the suction will result in the loss of fine-grained dense particles. Therefore, the authors are currently conducting additional studies on the initial feed with a variety of sizes and densities.

4.2. validation

To validate the model and simulation method, Viduka's work was used [4,5]. In the Viduka's articles, fluid flow in the CFD has been solved in two-dimensional (2D) mode using Ansys CFX, and only one cell in the thickness direction has been used to solve the fluid field. The DEM modelling of particles based on an in-house code has been considered three-dimensional (3D), while the thickness of the bed is equal to five particle diameters. The particles in the Viduka's articles are monodispersed (1 cm) and have two densities (2540 and 2630 kg/m3).

In the present study, both fluid flow modelling (CFD) and particle modelling (DEM) are conducted in a fully three-dimensional (3D) manner, with variations in the size and density of the particles (multi-size and multi-density). As evident from Fig. 13, in the case of the data from the Viduka article, although the numerical simulation methods employed in two papers differ, they exhibit similarities in particle trajectories and the number of cycles (four cycles) for separation. The results obtained from both simulation methods closely align. The observed discrepancy in particle height is deemed acceptable and could be attributed to the choice of a three-dimensional mode for both fluid and solid phases, as opposed to the reference article [4,5] where the fluid phase is two-dimensional, and the solid phase is three-dimensional. Alternatively, this difference may arise from variations in the software utilized in two articles.

5. Conclusion

The CFD and DEM coupling was utilized to check the removal of suction in the oscillating jig system. The results showed that the normal sinusoidal mode requires less cycle time than the complete suction removal mode. The amplitude of normal sinusoidal mode was more than twice the amplitude of velocity in the optimal mode with complete removal of suction. Further, in the optimal mode with complete removal of suction, the hutch water velocity was equivalent to the amplitude of its velocity function. Therefore, in case of complete removal of suction,

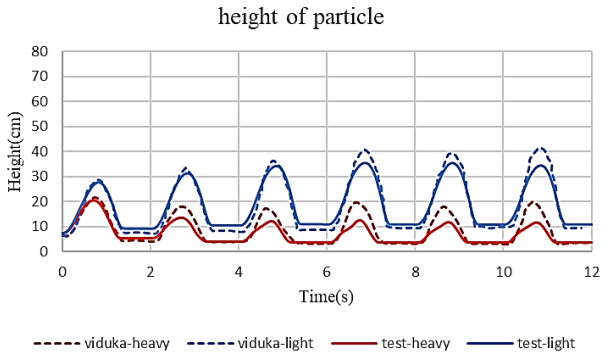

Figure 13. The average height of the particles in the reference article [17,18] and current article.

the velocity amplitude and hutch water velocity were lower than the velocity amplitude in the normal sinusoidal mode. The energy consumption for the optimal mode (which has a lower velocity amplitude and hutch water velocity) was significantly lower than the other modes. Therefore, we can qualitatively check and compare the amount of energy consumption for jigging. The limitations of the present work include the number of particles, as increasing it would rise the computational cost. In the future work, industrial conditions, such as different sin waves for each size range and feeds with different particle shapes will be tested. Moreover, the qualitative investigation of energy consumption in gravity concentration by the two-way CFD-DEM coupling simulation will be studied for feed segregation into different states and comparing them.

Acknowledgments

The authors are grateful to the Central Complex Laboratory, University of Kashan, and the Ultrafast Processing and Computing Center.

REFERENCES

[1] Wills, B.A. and J. Finch. 2015. Wills' Mineral Processing Technology, 8th ed. https://doi.org/10.1016/C2010-0-65478-2.

[2] Pryor, E. J. (1965). Mineral processing. Elsevier Publishing Co. Ltd. Amsterdam – London – New York, Chapter 13, 304-305.

[3] Constant, M., Coppin, N., Dubois, F., Artoni, R., Lambrechts, J., & Legat, V. (2021). Numerical investigation of the density sorting of grains using water jigging. Powder Technology, 393, 705–721. doi: https://doi.org/10.1016/j.powtec.2021.07.036

[4] Viduka, S. M., Feng, Y. Q., Hapgood, K., & Schwarz, M. P. (2013). CFD-DEM Investigation of Particle Separations using a Sinusoidal Jigging Profile. Advanced Powder Technology, 24, 328-342. doi: https://doi.org/10.1016/j.apt.2012.11.012

[5] Viduka, S. M., Feng, Y. Q., Hapgood, K., & Schwarz, M. P. (2013). Discrete particle simulation of solid separation in a jigging device. International Journal of Mineral Processing, 123, 108–119. doi: https://doi.org/10.1016/j.minpro.2013.05.001

[6] Srinivasan R., B.K. Mishra, and S.P. Mehrotra. 1999. Simulation of particle stratification in jigs. Coal Preparation 20(1-2):55–70. doi:10.1080/07349349908945592

[7] Mayer F.W. 1964. Fundamentals of a potential theory of the jigging process. 7th International Mineral Processing Congress 7:75–97.

[8] Tavares L.M., and R.P. King. 1995. A useful model for the calculation of the performance of batch and continuous jigs. Coal Prep. 15:99–128. doi:10.1080/07349349508905291

[9] Beck A.J.G., and P.N. Holtham. 1993. Computer simulation of particle stratification in a two-dimensional batch jig. Mineral Engineering 6(5):523–532. doi:10.1016/0892-6875(93)90179-Q

[10] Fatahi M.R., and A. Farzanegan. 2017. DEM simulation of laboratory Knelson concentrator to study the effects of feed properties and operating parameters. Advanced Powder Technology 28(6):1443–1458. doi:10.1016/j. apt.2017.03.011

[11] Mishra B.K., and S.P. Mehrotra. 1998. Modelling of particle stratification in jigs by the discrete element method. Mineral Engineering 11(6):511–522. doi:10.1016/S0892-6875(98)00033-8

[12] Mishra B.K., and S.P. Mehrotra. 2001. A jig model based on the discrete element method and its experimental validation. International Journal of Mineral Processing 63(4):177–189. doi:10.1016/S0301-7516(01)00053-9

[13] Mukherjee A.K., and B.K. Mishra. 2006. An integral assessment of the role of critical process parameters on jigging. International Journal of Mineral Processing 81(3):187–200. doi:10.1016/j. minpro.2006.08.005

[14] Mukherjee A.K., and B.K. Mishra. 2007. Experimental and simulation studies on the role of fluid velocity during particle separation in a liquid–solid fluidized bed. International Journal of Mineral Processing 82(4):211–221. doi:10.1016/j. minpro.2006.11.006

[15] Solnordal C.B., T. Hughes, S. Gray, and P.M. Schwarz. 2009. CFD Modelling of a Novel Gravity Separation Device. 7th International Conference on CFD in the Minerals and Process Industries, CSIRO Melbourne Australia 9-11.

[16] Xia Y.K. 2007. Applications of Computational Fluid Dynamics (CFD) Tools for Gravity Concentrators in Coal Preparation. Chemical Product and Process Modeling 2(1). doi:10.2202/1934-2659.1028

[17] Xia Y.K., and F.F. Peng. 2007. Numerical simulation of behavior of fine coal in oscillating flows. Mineral Engineering 20:113–123. doi:10.1016/ j. mineng.2006.06.004

[18] Xia Y.K., F.F. Peng, and E.Wolfe. 2007. CFD simulation of fine coal segregation and stratification in jigs. International Journal of Mineral Processing 82: 164–176. doi:10.1016/ j. minpro.2006.10.004.

[19] Asakura K., M. Mizuno, M. Nagao, and S. Harada. 2007. Numerical simulation of particle motion in a jig separator. 5th Joint ASME/JSME Fluids Engineering Conference, San Diego, California USA. Volume 1:385-391. doi:10.1115/FEDSM2007-37158

[20] Dong K.J., S.B. Kuang, A. Vince, T. Hughes, and A.B. Yu. 2010. Numerical simulation of the in-line pressure jig unit in coal preparation. Mineral Engineering 23(4):301–312. doi:10.1016/j. mineng.2009.10.009

[21] Tavares L.M. 1999. Monte Carlo simulations on the potential energy theory of jigging. Coal Prep. 20:71–83. doi:10.1080/07349349908945593

[22] Panda L., A.K. Sahoo, A. Tripathy, S.K. Biswal, and A.K. Sahu. 2012. Application of artificial neural network to study the performance of jig for beneficiation of non-coking coal. Fuel 97:151–156. doi:10.1016/ j. fuel.2012.02.018

[23] Ahmed M.M. 2011. Optimization of a jigging process using statistical technique. International Journal of Coal Preparation and Utilization 31:112–123. doi:10.1080/19392699.2010.549383

[24] Shuai, L., Runquan, Y., Caili, W., Yang, S., & Huaifa, W. (2022).

Simulation of the solid particles behavior in 3D stirred tank using CFD-DEM coupling approach. Particulate Science and Technology, 40(8), 911–21. doi: https://doi.org/10.1080/02726351.2021.2025179

[25] Che, H., Werner, D., Seville, J., Wheldon, T. K., & Windows-Yule, K. (2023). Evaluation of coarse-grained CFD-DEM models with the validation of PEPT measurements. Particuology, 82, 48–63. doi: https://doi.org/10.1016/j.partic.2022.12.018

[26] Razavi F., A. Komrakova, and C.F. Lange. 2021. CFD–DEM Simulation of Sand-Retention Mechanisms in Slurry Flow. Energies 14(13):3797. doi:10.3390/en14133797

[27] Di Felice R. 1994. The voidage function for fluid–particle interaction systems. International Journal of Multiphase Flow 20(1):153–159. doi:10.1016/0301-9322(94)90011-6

[28] ESSS Rocky. 2021. Release 4.5.2, User Manual, ESSS Rocky DEM, S.R.L

[29] Kolahi, S., Jahani-Chegeni, M., & Seifpanahi-Shabani, K. (2021). Investigation of the effect of industrial ball mill liner type on their comminution mechanism using DEM. International journal of mining and geo-engineering, 55(2), 97-107. doi: https://doi.org/10.22059/IJMGE.2020.289423.594826

[30] Ansys, (2021). Release 2021 R2, Ansys Fluent Theory Guide.

[31] Alobaid, F., Baraki, N., and B. Epple. 2014. Investigation into improving the efficiency and accuracy of CFD/DEM simulations. Particuology, 16, 41-53. doi:10.1016/ j. partic.2013.11.004.

[32] Crespo E.F. 2016. Modeling segregation and dispersion in jigging beds in terms of the bed porosity distribution. Mineral Engineering 85:38–48. doi:10.1016/j. mineng.2015.10.012